Journal of Petroleum Exploration and Production Technology
https://doi.org/10.1007/s13202-024-01793-9

ORIGINAL PAPER-PRODUCTION ENGINEERING

Effect of equilibrium contact angle on water equilibrium film thickness for the carbon dioxide–brine–mineral system based on surface force theory

Mumuni Amadu[1] · **Adango Miadonye**[1]

Received: 14 October 2022 / Accepted: 16 March 2024

Abstract

The thickness of the thin wetting film depends on disjoining pressure forces, and it evolves with pH evolution due to brine acidification at the physical and chemical conditions of geological carbon dioxide storage becoming thinner in response to dewetting. In the literature, molecular dynamic simulation (MDS) studies have been employed to understand the effect of pressure/capillary pressure on the thin wetting film evolution. In this paper, a theoretical approach based on the Frumkin–Derjaguin Equation (FDE), models of electric double layer repulsion, and van der Waals forces have been used for the calculation of the wetting film thickness. The approach excluded hydration forces contribution to disjoining pressure forces due partly to its poorly understood nature, and partly to the high salinity conditions encountered in geological carbon storage. Due to its promising global storage capacity compared to other lithologies, the carbon dioxide–brine–silica systems was chosen to simulate sandstone saline aquifers. The validation of the model benefited much from literature resources on data and a universal model of carbon dioxide–brine interfacial tension. Calculated results confirm pH-induced dewetting and they follow trends controlled by pH and pressure as found in the literature. The novelty of the paper can be seen from the fact that it has demonstrated a theoretical supplement to MDS studies in addition to justifying the fundamental utility and versatility of the FDE. Moreover, the paper links for the first time, a transcendental equation to the thin wetting film theory encountered in the carbon dioxide–solid–brine system found in geological carbon storage.

Keywords Contact angle · Thin wetting film · Hamaker constant · Interfacial tension · Salinity · Debye length scale

List of symbols

(A_{123})	Hamaker constant for a system where phase 1 and phase 2 are interacting through phase 3
A_0	Pressure and temperature dependent constants.
B_0	Pressure and temperature dependent constants
$a(N)$	Parameter defined by Eq. (20)
A_D	Constant approximately equal to 0.5
C	Concentration [moles/m^3]
e	Electronic charge [C]
h	Film thickness
h'	Planck's constant
h_0	Equilibrium film thickness
I	Ionic strength [M]
k_B	Boltzmann constant
K_{CA}^1	First dissociation constant of carbonic acid [M]
m_{CO_2}	The solubility of carbonic acid [M]
m	Mol.kg^{-1} associated with Eq. (22)
N	Normality [N]
N_A	Avogadro's number [number of particles per mole] and C is the concentration [moles/m^3]
pH	Logarithm to base of the hydrogen ion concentration
pH_{pzc}	Point of zero charge pH
T	Temperature [K]
n_i	Refractive index of material i
T	Temperature in Kelvin

Greek letters

α	Gas phase
β	Solid phase
γ	Brine phase
$\sigma^{\alpha\beta}$	Interfacial tension between α. and β phases[mN m^{-1}]
γ_a	Activity coefficient

✉ Mumuni Amadu
Mumuni_amadu@cbu.ca; mumuniamadu@hotmail.com

Adango Miadonye
Adanfo_miadonye@cbu.ca

[1] School of Science and Technology, Cape Breton University, P. O. Box 5300, Sydney, NS, Canada

Published online: 23 April 2024

ε_i	Relative permittivity of material i
ε_0	Permittivity of free space [Fm^{-1}]
ζ_M	Zeta potential for water containing monovalent
$\varepsilon_0(T,0)$	Dielectric permittivity of pure water as function of temperature and ze salinity [Fm^{-1}]
$\varepsilon(T,N)$	Dielectric constant of brine as a function of temperature and salinity (normality) [Fm^{-1}]
ε_r	Relative permittivity [–]
θ	Thermodynamic/equilibrium contact angle [°]
v_e	Main electronic absorption frequency [Hz]
$\sigma^{\alpha\beta}$	Interfacial tension between α and β phases
π	Disjoining pressure as a function of film thickness [nm]
π_{ell}	Electrical or double layer disjoining pressure [pas]
κ	Inverse of Debye length [nm]
λ_D	Characteristic distance for potential decay due to screening
ψ^1_{eff}	Surface potential of interface 1 [V]
ψ^2_{eff}	Surface potential of interface 2

Introduction

The thickness of the wetting film on a solid surface is a parameter of immense thermodynamic significance that matters in several industrial operations. For instance, in tribology, bubbles rubbing on a solid surface was investigated using interferometry based on a unique experimental setup that enabled monitoring the thickness profiles of a wetting film located between the bubble and a hydrophilic glass surface (Karakashev et al. 2014). In the cited study, determination of the 3D film thickness profiles allowed calculation of 3D maps over the wetted surface, which give a clue regarding efficiency of lubrication or the zero friction concept (Radoev et al. 2007a, b). Still on tribology, knowledge of thin wetting film thicknesses variation over solid surfaces has been used to decipher surface heterogeneity in lubrication issues (Radoev et al. 2007a, b). In the coating industry, the thickness of the wetting film is used as a critical guide to calculating the dry wetting film that is supposed to provide fire proof/corrosion resistance of coated surfaces (IFTI 2018). In colloidal dispersion systems, compression of the electric double layer due to the addition of salts is the principal cause of double layer contraction which reduces wetting film thickness. For such systems, enhancing dispersion stability has been achieved, using stabilization by addition of Hydrophobically Modified Inulin Polymeric Surfactant (Exerowa et al. 2009), where direct measurement of the wetting film thickness can prove as an indication of surfactant efficiency.

Within the framework of the Derjaguin–Landrup–Verwey–Ovebeek (DLVO) theory, the thermodynamic basis of the thin wetting film has been extensively explored. In this regard, principal to the thermodynamics of the equilibrium wetting film is the quantitative interpretation of disjoining pressure, which controls film stability (Bergeron 1997; Kuchin et al. 2014). The disjoining pressure is a physical quantity interpreted as the pressure needed to separate two parallel plates from each other when there is an intervening liquid phase (Condon 2006). It has electrostatic, van der Waals, and non-DLVO contributions in the form of hydration pressure (Altamirano et al. 2016). In all three contributions, disjoining pressure is a function of wetting film thickness. Therefore, a precise measurement of disjoining pressure permits calculation of film thickness. For instance, disjoining pressure has been measured using a microfabricated groove for a molecularly thin polymer liquid film on a solid surface (Fukuzawa et al. 2004a, b), by combining a thin-film balance with AC impedance spectroscopy (Yaros et al. 2003), and using atomic force microscopy technique (Jones et al. 2005; Bowles et al. 2009; Hamilton et al. 2010). Atomic force microscope has also been used to characterize the nanoscale surface water films on mica surface exposed to deep ground waters (Gaebel et al. 2009).

Geological storage of anthropogenic carbon dioxide is expected to isolate large quantities of the gas compared to other sequestration options due to the promising global storage potential (Verma et al. 2021). However, while the storage potential is attractive, water–rock interaction phenomenon that controls wettability, and the distribution of sub-surface fluid phases (brine and dioxide) is less understood. In this regard, the dissolution of injected carbon dioxide under saline aquifer temperature, pressure and salinity conditions and the consequence interaction of the dissolved species with aquifer minerals will result in rock–brine interfacial free energy evolution. The implication, considering the Young's equation, is the change in contact angle/wettability due to pH decrease (Kim et al. 2012). Therefore, to understand the effect of wettability evolution on the relative mobility of subsurface fluids (Sun and Bourg 2020), which impacts gas injection and storage efficiency under supercritical conditions, quantification of the water–rock interaction effect by experimental means is necessary. Moreover, the two-phase flow of injected carbon dioxide and resident formation brine implies the existence of the carbon dioxide–brine and brine–solid interface, where disjoining pressure (Kim et al. 2012) plays a central role in dewetting issues. Therefore, the DLVO theory must provide a theoretical basis for the determination of equilibrium film thickness like those mentioned earlier. In this regard, the Frumkin–Derjaguin (FD) equation that links the thermodynamic contact angle and the integral of disjoining pressure is an attractive and robust mathematical resource for the determination of wetting film thickness, given the dependence of disjoining

pressure on it. While the approaches mentioned earlier rely on direct measurement of disjoining pressure to calculate film thicknesses from van der Waals and electrostatic models, the application of the FD equation facilitates film thickness determination by integration of experimentally measured thermodynamic/equilibrium measured contact angle. However, while this approach is feasible, no research work in geological carbon storage has so far been devoted to it, apart from research works on molecular dynamic simulations (Sun and Bourg 2020; Tenney and Cygan 2014; Liu et al. 2021; Hamm et al. 2013; Chen et al. 2016). For instance, used molecular dynamics simulation to demonstrate the microscopic wetting behavior of two solid model surfaces for the first time, where the effect of contact angle on wetting/thin film was highlighted. Sun and Bourg (2020) simulated water and CO_2 at various pressures between quartz surfaces to probe the thickness of the adsorbed water film observed between the CO_2 and quartz surface, and the radius of curvature of the fluid–fluid interface as a function of CO_2 pressure. Their results were discussed in the context of the relevant interfacial energies, Young's equation, and the Gibbs CO_2 surface excesses at various interfaces. Hamm et al. (2013) used MD simulation to examine fundamental wetting and capillary properties for the system quartz–water–scCO_2 systems at a range of pressures where disjoining pressure effect on the wetting film was fundamental in the simulation process.

Different types of saline aquifers occur in nature, but those of sandstone origin provide the greatest global storage capacity (William et al. 2016) with promising global distribution and favorable compressibility (Verma et al. 2021). Similar to Badera et al. (2014). The carbon-dioxide-sandstone systems were chosen in the study due to its acclaimed global potential for anthropogenic carbon dioxide storage. Herein, models of the electric double layer and van der Waals disjoining pressure components have been substituted into the FD equation. Accordingly, integration of the resulting equation within the limits set by the original FD equation leads to a transcendental equation that expresses contact angle as a function of film thickness at a given pH, temperature and salinity of the system. Determination of film thicknesses under carbon dioxide pressure induced dewetting conditions was then carried out based on literature experimentally measured equilibrium contact angles for the system carbon dioxide–brine–solid systems under in-situ conditions of geological carbon storage. Results of equilibrium film thicknesses correlate with dewetting trends reported in the literature. The novelty of this work is judged by its rigorous derivation of the relationship between equilibrium contact angle and equilibrium film thickness by integrating models of disjoining pressure in the DLVO theory and models of surface potentials in the electrochemical literature into the original FD equation. It serves as a supplementary research work to those of Kim et al. (2012) involving direct measurement of wetting film on a mineral surface and Shiga et al. (2020), who used the FD equation to study the effect of pressure on total disjoining pressure and molecular dynamics simulation findings. In this regard, this paper has demonstrated that theoretical determination of thin wetting film thickness follows experimentally observed trends in the literature. In addition, the paper links for the first time, a transcendental equation to the thin wetting film encountered in geological carbon storage.

Theoretical development

Contact angle: film thickness relationship

If carbon dioxide is injected into a saline aquifer, a two-phase flow regime evolves where a gas-formation brine–solid system forms with a gas–brine interface and a brine–solid interface. Following the existence of the electric double layers at the interfaces, double layer repulsion will provide electrostatic contribution to disjoining pressure. Besides, van der Waals forces will also provide molecular interaction contribution to disjoining pressure as will hydration forces interactions. As gas phase increases, the system pressure increases such that at a given pressure, equilibrium film thickness exists. In addition, dissolution of carbon dioxide will cause water–rock interaction at the solid–liquid interface as pH evolves. Such a system can be described by the following schematic given in Fig. 1 (Hirasaki 1991).

α is the gas phase γ is the brine phase, β is the solid phase, h_0 is the equilibrium film thickness, θ is the thermodynamic/equilibrium contact angle and $\sigma^{\alpha\beta}$ [mN m^{-1}] is the interfacial tension between α and β phases.

A practical approach to calculating van der Waals forces is derived from Lifshitz' theory, where rather than treating the total van der Waals energy as a sum of pairwise interactions between atoms, the theory considers component materials as continua with electromagnetic fluctuations at all frequencies (Ninham and Parsegian 1970). However, the limitation imposed by the assumption of dielectric continuum is seen where change in molecular structure at the solid–liquid interface due to electrostatic (surface charge) phenomena results in changes in the dielectric permittivity at the interfacial region. In this paper, the focus is on geological storage of anthropogenic carbon dioxide in deep saline aquifers, where salinity conditions minimize the electrostatic effect due to the dependence of zeta potential on pH and salinity (Hirasakl 1991), which merits the application of the Frumkin–Derjaguin equation without accounting for structural forces contribution to disjoining pressure.

Based on the schematic seen in Fig. 1, a robust thermodynamic model, the Frumkin–Derjaguin equation, provides a fundamental relationship in the theory of thin films and

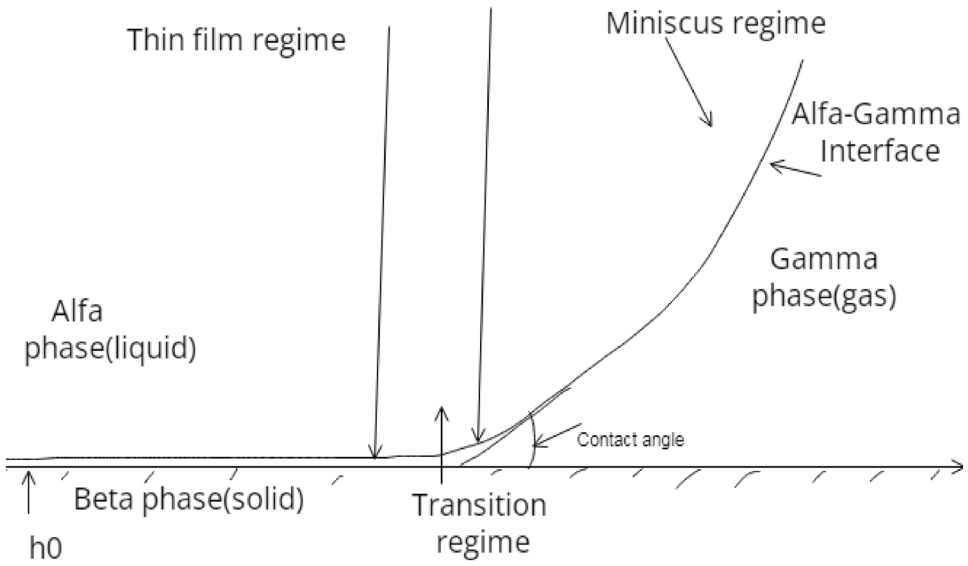

Fig. 1 Schematics of the equilibrium film thickness (Hirasaki 1991)

relates all surface tensions between surfaces associated with a wetting film to its disjoining pressure and contact angle (Rusanov 2020). The equation reads (Hirasaki 1991).

$$1-\cos\theta=\left[-\int_{h_o}^{\infty}\pi \mathrm{d}h-h_o\pi\left(h_o\right)\right]\Big/\sigma^{\gamma\beta} \tag{1}$$

In Eq. (1), π is the disjoining pressure as a function of film thickness h. All other parameters have been explained.

Van der Waals forces contribution to disjoining pressure is given as (Misra et al. 2019):

$$\pi_{vdw}=-\frac{A_{\mathrm{H}}}{6\pi h^3} \tag{2a}$$

In this equation, A_{H} is Hamaker constant [J], h. is film thickness [nm] and π is 3.14.

The coefficient A, of the van der Waals disjoining pressure is the Hamaker constant, which quantifies the extent of intermolecular interaction. For values greater than zero, the interaction is attractive in nature. The Hamaker constant of CO_2 and H_2O can be calculated from the Lifshitz theory, using experimental data on refractive indices and the relative permittivities. Generally, A_{ii} means the constant for a material i interacting across a vacuum and it is given as (Shiga et al. 2020):

$$A_{ii}=\frac{3k_{\mathrm{B}}T}{4}\left(\frac{\varepsilon_i-1}{\varepsilon_i+1}\right)^2+\frac{3h'v_e\left(n_i^2-1\right)^2}{16\sqrt{2}\left(n_i^2+1\right)^{3/2}} \tag{2b}$$

where k_{B}. is the Boltzmann constant, T is the temperature, ε_i. is the relative permittivity of material i, h' is the Planck's constant, v_e is the main electronic absorption frequency, n_i is the refractive index of material i, and the material numbers of minerals, CO_2, and H_2O are 1, 2, and 3, respectively. The Hamaker constant of the water film sandwiched between the CO_2 phase and the mineral phase (A_{123}) is calculated from A_{11}, A_{22}, and A_{33} based on the mixing rule as:

$$A_{123}=A_{12}+A_{33}-A_{13}=\left(\sqrt{A_{11}}-\sqrt{A_{33}}\right)\left(\sqrt{A_{22}}-\sqrt{A_{33}}\right) \tag{2c}$$

When the surfaces are sufficiently far apart, the potential profiles originating from each individual surface will not be much perturbed by the presence of the other surface, which permits the application of superposition theory to the derivation of double layer repulsion disjoining pressure. In this paper, the model based on superposition will be adopted because of its application to asymmetric systems. The equation reads (Ohshima 2014; Evans and Wennerstöm 1999):

$$\pi_{\mathrm{el}}=2\varepsilon\varepsilon_o\kappa^2\psi_{\mathrm{eff}}^1\psi_{\mathrm{eff}}^2e^{-\kappa h} \tag{3}$$

In this equation, π_{ell} is the electrical or double layer disjoining pressure, ε_{r} is relative permittivity [–], ε_0 is permittivity of free space [Fm],κ is the inverse of Derbye length [nm], ψ_{eff}^1 is the surface potential of interface 1 [V], and ψ_{eff}^2 [V] is the surface potential of interface 2.

The focus is on geological carbon storage in saline aquifers, where salinities are supposed to be high, and in excess of 10,000 ppm (Evans and Wennerstöm 1999; Kelemen et al. 2019). Under such condition, extension of the classical DLVO theory by adding hydration forces disjoining pressure component is unnecessary, as it becomes important only at moderate or low salinities (Boström et al. 2001). Therefore, total disjoining pressure based on the classical DLVO theory will be adopted in this work. Substitution of Eqs. (2a) and (3) into Eq. (1) gives:

$$1-\cos\theta=\left[\int_{h_o}^{\infty}\left(-\frac{A_{\mathrm{H}}}{6\pi h^3}-2\varepsilon\varepsilon_o\kappa^2\psi_{\mathrm{eff}}^1\psi_{\mathrm{eff}}^2e^{-\kappa h}\right)\mathrm{d}h-h_o\pi\left(h_o\right)\right]\Big/\sigma^{\gamma\beta} \tag{4}$$

Integration gives the first two terms on the right-hand side of Eq. (4) as:

$$\left(0.25\frac{A_{\mathrm{H}}}{\pi h_0^2}-2\varepsilon\varepsilon_o\kappa\psi_{\mathrm{eff}}^1\psi_{\mathrm{eff}}^2e^{-\kappa h_o}\right)\Big/\sigma^{\gamma\beta} \tag{5}$$

Writing the last term of Eq. (4) in terms of equilibrium film thickness and its addition to the result of integration gives:

$$1-\cos\theta=\left(0.25\frac{A_{\mathrm{H}}}{\pi h_0^2}-2\varepsilon\varepsilon_o\kappa\psi_{\mathrm{eff}}^1\psi_{\mathrm{eff}}^2e^{-\kappa h_o}\right)\Big/\sigma^{\gamma\beta}-h_o2\varepsilon\varepsilon_o\kappa^2\psi_{\mathrm{eff}}^1\psi_{\mathrm{eff}}^2e^{-\kappa h_o}/\sigma^{\gamma\beta} \tag{6}$$

The Debye length, λ_D is the characteristic distance for potential decay due to screening (Kesler et al. 2020) and its reciprocal κ is given as (Waggett et al. 2018):

$$\kappa=\frac{1}{\lambda_D}=\left(\frac{\varepsilon_0\epsilon_{\mathrm{r}}k_{\mathrm{B}}T}{e^2N_{\mathrm{A}}2C}\right)^{-1/2} \tag{7}$$

where N_{A} is Avogadro's number [number of particles per mole] and C is the concentration [moles/m^3], T is the temperature in Kelvin, and e is the electronic charge [C].

Using Nernst equation, the surface potential of solid surface can be written as (Amadu and Miadonye 2019a, b):

$$\Psi_o=\frac{2.3RT}{F}\left(\mathrm{pH}_{\mathrm{pzc}}-\mathrm{pH}\right) \tag{8}$$

In Eq. (8), R is the universal gas constant [J K^{-1}], F is Faraday constant [C mol^{-1}], $\mathrm{pH}_{\mathrm{pzc}}$ is the pint of zero charge pH of surface and pH is the negative logarithm to base 10 of the hydrogen ion concentration.

Assuming the potential of carbon dioxide–brine interface can be denoted by phase 1 and that between-brine and solid surface by phase 2, the following potentials can be written for the interfaces:

$$\psi_{\mathrm{eff}}^1=\frac{2.3RT}{F}\,\mathrm{pH} \tag{9}$$

$$\psi_{\mathrm{eff}}^2=\frac{2.3RT}{F}\left(\mathrm{pH}_{\mathrm{pzc}}-\mathrm{pH}\right) \tag{10}$$

Equation (9) was obtained from Eq. (8) based on the assumption that the point of zero charge pH is characteristic of a solid surface and must be zero for the carbon dioxide–brine interface, given that this interface is different from that of crude oil–brine interface where, the point of zero charge pH is important (Bonto et al. 2019).

Substitution of Eqs. (9) and (10) into Eq. (6) gives:

$$1-\cos\theta=\left(0.25\frac{A_{\mathrm{H}}}{\pi h_0^2}-2\varepsilon\varepsilon_o\kappa\left(\frac{2.3RT}{F}\right)^2\left(\mathrm{pH}_{\mathrm{pzc}}-\mathrm{pH}\right)(-\mathrm{pH})e^{-\kappa h_o}\right)\Big/\sigma^{\gamma\beta}-h_o2\varepsilon\varepsilon_o\kappa^2\left(\frac{2.3RT}{F}\right)^2\left(\mathrm{pH}_{\mathrm{pzc}}-\mathrm{pH}\right)(-\mathrm{pH})e^{-\kappa h_o}/\sigma^{\gamma\beta} \tag{11}$$

At a given pH of aqueous solution defined by pressure, temperature and salinity, Eq. (11) gives an explicit relationship between the thermodynamic contact angle and the equilibrium film thickness. Geologically, rock is an aggregate of minerals (Nesse 2000). Therefore, to understand the water–rock interaction effect on wettability evolution during CO_2 injection into saline aquifers, rock forming minerals have been interacted with dissolved carbon dioxide species under temperature, pressure and salinity conditions of geological storage (Shiga et al. 2020, 2012; Jung and Wan 2011; Saraji et al. 2013), thus, experimental data on contact angle versus pressure at specified temperatures and salinities will permit the theoretical determination of the equilibrium film thickness, using Eq. (11). To achieve the objective, additional task is required to determine pH at specified temperature, pressure and salinity conditions. The following section discusses the additional task involved.

Auxiliary equations

Given carbon dioxide solubility dependence on temperature, pressure and salinity (Yan et al. 2011), the pH of aqueous solution is a function of temperature, pressure and salinity. Therefore, an equation is needed to calculate carbon dioxide solubility at a given pressure, temperature and salinity. Besides, an equation is needed to calculate the dissociation of dissolved and hydrated carbon dioxide in the form of carbonic acid. Such an equation provides the basis for the calculation of hydrogen ion concentration at a given temperature, pressure and salinity which is needed to calculate film thickness in Eq. (11).

Bahadori et al. (2009) have developed a correlation for predicting the solubility of carbon dioxide in pure water

as well as in aqueous sodium chloride solutions based on reduced variables of temperature and pressure, and thermodynamic interaction parameters. They applied the solubility model to correlate carbon dioxide solubilities in aqueous solutions for temperatures between 300 and 400 K and for pressures from 50 to 700 bars, with good agreement between predicted and experimental data. Their solubility model is given as:

$$x = a + bP_r + CP_r^2 + dP_r^3 \tag{12}$$

where

x is carbon dioxide solubility-mol L^{-1}

$$\begin{aligned} a &= A_1 + B_1T_r + C_1T_r^2 + D_1T_r^3 \\ b &= A_2 + B_2T_r + C_2T_r^2 + D_2T_r^3 \\ c &= A_3 + B_3T_r + C_3T_r^2 + D_3T_r^3 \\ d &= A_4 + B_4T_r + C_4T_r^2 + D_3T_r^3 \end{aligned} \tag{13}$$

The dissolution of carbon dioxide in brine will produce hydrogen ions. Assuming experimental brines were prepared using deionized water, the initial concentration of hydrogen ions will be negligible compared to that given by the dissociation reaction. Therefore, the pH of the brine can be calculated as (Amadu and Miadonye 2019a, b):

$$\mathrm{pH} = \log\left(\gamma \frac{K^1_{\mathrm{CA}} \pm \sqrt{\left(K^1_{\mathrm{CA}}\right)^2 + 4K^1_{\mathrm{CA}} m_{\mathrm{CO_2}}}}{-2}\right) \tag{14}$$

The activity coefficient model is given as (Stumm and Morgan 1996):

$$\log\left(\gamma_a\right) = -A_{\mathrm{D}} z^2 \left[\frac{I^{1/2}}{I + I^{1/2}} - 0.2I\right] \tag{15}$$

where γ_a is the activity coefficient, A_{D} is a constant approximately equal to 0.5 and z is the valence on the ion.

I is the *ionic strength* (mol/liter) of the aqueous solution, defined as follows (Kennedy 1990):

$$I = \sum_i^n \left(z_i\right)^2 C_i \tag{16}$$

where z_i is the charge number on each ion in the solution, and C_i is the concentration of each ion (mol/liter).

The salinity and temperature dependence of the first ionization constant of carbonic acid formed by the dissolution and hydration of carbon dioxide (Reddi 2011) is given as (Aissa et al. 2015):

$$\begin{aligned} \ln K^1_{\mathrm{CA}}(\mathrm{TS}) = {} & \frac{2936978}{T^2} + \frac{17883}{T} - 41.489 \\ & + \left(\frac{1141179}{T^2} - \frac{17883}{T} + 13.40776\right)\sqrt{I} \\ & - 1.414245I + 0.2677258I^{3/2} \end{aligned} \tag{17}$$

To calculate κ, which is the reciprocal of Debye length using Eq. (7), the relative permittivity of brine at the specified temperature is required. Stogryn (1971) has published an empirical correlation for calculating the dielectric permittivity. In this regard, the dielectric permittivity of brine as a function of temperature and salinity is given as:

$$\varepsilon_0(T, N) = \varepsilon_0(T, 0)a(N) \tag{18}$$

In this equation, $\varepsilon(T, N)$ is the dielectric constant of brine as a function of temperature and salinity (normality).

$\varepsilon_0(T, 0)$ is the dielectric permittivity of pure water as function of temperature and zero salinity defined by the following relation (Malmberg and Mariyott 1965):

$$\varepsilon_0(T, 0) = 87.74 - 0.40008T + 9.398 * 10^{-4}T^2 + 1.410 * 10^{-6}T^3 \tag{19}$$

$a(N)$ is defined as:

$$a(N) = 1.000 - 0.2551N + 151 * 10^{-2}N^2 - 6.889 * 10^{-3}N^3 \tag{20}$$

The salinity contribution (N) is defined as:

$$N = S(1.707 * 10^{-10} + 1.205 * 10^{-5}S + 4.058 * 10^{-9}S^2) \tag{21}$$

Interfacial tension correlation

In addition to the auxiliary equations required for calculation of related parameters in Eq. (11), knowledge of interfacial tension for the carbon dioxide–brine system at specified conditions of temperature, pressure and salinity is essential. Li et al., (2012) have developed an empirical correlation for the CO_2–brine system. Experimental measurements were conducted at temperatures between (298 and 473) K at varying pressures up to 50 MPa, using salinity range (1–5 mol kg^{-1}) by means of imaging a pendant drop of CO_2-saturated brine surrounded by a water-saturated CO_2 phase. The uncertainty at 95% for interfacial tension is between 0.016 and 0.6 mN m^{-1} (Li et al. 2012). It is applicable over temperature range (from 25 to 175 Celsius) and a pressure range (from 2 to 50 MPa). The following gives the correlation:

$$\sigma^{\alpha\beta} = A_0 m + B_0 \tag{22}$$

In this equation, A_0 and B_0 are pressure and temperature dependent constants defined in the paper by Li et al. (2012). The unit of m is mol kg^{-1}. The correlation was used for calculating interfacial tensions.

Several researchers have studied the effect of temperature, pressure and salinity on the interfacial tension between carbon dioxide and brine at geological conditions characteristic of the saline aquifer (Aggeloppous et al. 2011; Chalbaud et al. 2009). The aim of Li et al. (2012) was to research the dependence of interfacial tension on temperature, pressure, and salinity over the range of conditions applicable to carbon dioxide storage in underground reservoirs with the principal objective of arriving at a universal model. Therefore, the universality of the model used in interfacial tension calculation in this research work does not warrant addressing salinity range limitations.

Equilibrium contact angle data

Several studies involving contact angle measurements on rock minerals have been reported in the literature. For instance, Jung and Wan (2012) have measured contact angles on silica for the system carbon dioxide–brine–silica to simulate carbon dioxide–water rock interaction effect on contact angle for sandstone saline aquifers (See Appendix 1). They reported contact angles for different salinities at 318 K. Chen et al. (2015), have also measured contact angles on silica for a molar sodium chloride brine at the same temperature (See Appendix 3). Jafari and Jung (2018), have also measured contact angle on mica, using a molar sodium chloride brine (See Appendix 2). To determine equilibrium film thicknesses using Eq. (11), pH values were calculated using Eq. (14) while solubilities values were calculated using Eq. (12). To achieve the objective, equilibrium contact angle data relating to the cited literature will be used for equilibrium thin film calculations based on Eq. (11).

Calculated parameters

The reciprocal of Debye length was calculated using Eq. (7). The ionization constant was calculated using Eq. (17). The value of the first ionization constant for carbonic acid in 1 M sodium chloride was calculated as 7.015×10^{-10}.

The ionic strength and activity coefficient were calculated using Eqs. (16) and (15), respectively. The value of activity coefficient is 0.71. The value of ionic strength for 1 M sodium chloride solution is 1. Regarding Jung and Wan (2012), the experimental data for 1 molar sodium chloride solution were used in this work. For Chen et al. (2015), the experimental data for sodium chloride (1 M) is found in Appendix 2. Table 1 gives calculated values of parameters of Eq. (11) and physical constants used.

The Hamaker constant for the system carbon dioxide–brine–solid was calculated using Eq. (2b).

The dielectric constant of silica was taken as 3.5, and its temperature dependence is weak (Jones 2005). The dielectric constant of mica was taken as 6.8 (Table 2 of (Zulkifli et al. (2017). The dielectric constant of carbon dioxide as a function of temperature and pressure was taken from Michels and Michels (1933), by extrapolating between plots for 40.26 and 49.76 °C (See Appendix 4).

The refractive of carbon dioxide and brine at 45 °C was calculated using the relationship between relative permittivity and dielectric constant as (Sebastian 2008)

$$\varepsilon_r = n^2 \tag{23}$$

In this work, the dielectric constant of sandstone for Chen et al. (2015) was assumed to represent a wet one and a median value of 7.5 was taken based on Daniels (1996) (Table 1).

Hamaker constants were calculated using Eqs. (2b) and (2c), using a value of $6.6 * 10^{-34}$ J s for Planck's constant (Stanford and Tanner 1985). Most absorption frequencies are in the ultraviolet region and a typical value of $3 * 10^{15}$ s^{-1} was taken as the absorption frequency (Israelachvili 2011), that was used in Hamaker constant calculation. Values were $0.46 * 10^{-20}$ for quartz in water

Table 1 Calculated values of parameters and values of physical constants used in the calculations

Parameter	Calculated value	Physical constants used	Value	Reference
$\kappa_{MNaCl}(m^{-1})$	33,420,177,596	Boltzmann constant [J K^{-1}]	$1.381 * 10^{-23}$	Chairman et al. (1942)
ε_{rMNaCl}	71.19	Electronic charge [C]	$1.602 * 10^{-19}$	Chairman et al. (1942)
ε_{rDW}	71.77	Avogadro's number [number per mol]	$6.022 * 10^{23}$	Chairman et al. (1942)
		Permittivity of free space ε_0 [Fm^{-1}]	$8.854 * 10^{-12}$	Chairman et al. (1942)

κ_{MNaCl}: reciprocal of Debye length scale for 1 M sodium chloride solution

ε_{rMNaCl}: relative permittivity for 1 M sodium chloride solution

ε_{rDW}: relative permittivity for deionised water

(Bergström 1997), 1.34 * 10^{-20} for mica (Bergström 1997) and 9.98 * 10^{-21} for 1 M sodium chloride brine. The dielectric constant of mica was taken as 6.4 (Weeks Jr. 1922). The dielectric constant of carbon dioxide as a function of pressure at 318 K was read from Appendix 4.

Results and discussion

The key parameters that determine the refractive index of a gas are the polarizability, temperature, and the pressure (Clergen et al. 1999). Among these, polarizability is determined by the gas itself. Temperature and pressure can be varied to determine their effect on the refractive index of a gas. Tables 2, 3 and 4 show calculated results of refractive index, using Eq. (23). In all cases, the refractive index calculated using the dielectric constant data from Appendix 4 increases with pressure for carbon dioxide, indicating decrease in the speed of light with pressure. In all systems, dielectric constant increases with pressure, consistent with the experimental results of Zhang et al. (2005), and also consistent with the virial equation for dielectric constant in terms of pressure and temperature (Kano and Kuramoto 2021).

The theoretical basis of this work hinges on the analytical derivation of a transcendental equation that describes the salinity, temperature, pH and contact angle dependent equilibrium film thickness for the carbon dioxide–brine–solid systems, exploiting the concept of disjoining pressure within the classical DVLO theory. Hydration forces are short-range interactions that act at a few nanometers on the mineral surface and are strongly dependent on the adsorption structure. Generally, the balance between hydration and DLVB forces at solid–liquid interfaces govern processes, such as colloidal stability, wetting, ion adsorption. etc. (Aram et al. 2022). However, the origin of molecular scale hydration forces and their implications for surface charge density that controls continuum scale electrostatic forces in such systems are poorly understood. Therefore, their contribution to total disjoining pressure used in the derivation of Eq. (11) was not considered. Moreover, hydration forces have been reported to decrease with high electrolyte concentration (Afzal et al. 1984) similar to that studied in the present work (1 M sodium chloride solution). In line with the objective of the study related to the equilibrium film thickness, the solution to equation Eq. (11) is necessary. In the mathematical literature, transcendental equations have been solved, using diverse mathematical tools. For instance, transcendental equations have been solved analytically (Perovich et al. 2014, 2007) numerically (Fiedler 1994), using artificial neural network (Jeswal and Chakraverty 2018) and using Cauchy's integral theorem for complex variables and transforms (Luck et al. 2015). In the present study a purely analytical method was used based on Maple version 15 developed by the University of Waterloo researchers. Tables 5, 6 and 7 show the solutions to the equilibrium film thickness equation as a function of pressure, interfacial tension, Hamaker constant and contact angle.

The Hamaker constant is a coefficient that relates the interactive van der Waals energy to the distance of separation between two molecules, where the interactive force is pair-wise additive and independent of the intervening media. Generally, the interactions between the particles are relative to the macroscopic properties of the dielectric constant, and the refractive index. Negative values of Hamaker constant arise where the dielectric permittivity of the intervening medium (brine) is between those of the interacting media (CO_2 and substrate) (Lee and Wolfgang 2001).

For Jung and Wan (2012) and Jafari and Jung (2018) experimental data, Hamaker constants are negative for pressures from 7 to 7.3 MPa and from 5 to 10 Mpa, respectively, decreasing in negative values. Therefore, van der Waals

Table 2 Calculated refractive index versus pressure for Jafari and Jung (2018) experimental data

Pressure-MPa	Dielectric constant	Refractive index
5.00	1.06	1.03
7.80	1.11	1.05
10.00	1.190	1.09
15.00	1.43	1.20

Table 3 Calculated refractive index versus pressure for 1 M sodium chloride solution for Jung and Wan (2012) experimental data

Pressure-MPa	Dielectric constant	Refractive index
7.00	1.105	1.05
7.25	1.107	1.05
7.30	1.108	1.05
15.00	1.401	1.18

Table 4 Calculated refractive index versus pressure for Chen et al. (2015) experimental data

Pressure-MPa	Dielectric constant	Refractive index
7.00	1.105	1.05
8.00	1.107	1.05
9.00	1.146	1.07
10.00	1.190	1.09
12.00	1.390	1.18
18.00	1.44	1.20

Table 5 Calculated equilibrium film thickness, interfacial tension and Hamaker constant based on Chen et al. (2015) experimental data

Pressure-MPa	Contact angle-degrees	Interfacial tension-mN/m	Hamaker constant-J * 10^{-20}	pH	Film thickness-nm
7	21.85	42.49	1.99	3.34	0.930
8	22.5	40.42	1.98	3.26	0.924
9	23	38.79	1.88	3.18	0.923
10	23.75	37.45	1.78	3.12	0.863
12	23.85	35.53	1.30	3.01	0.754
18	23.92	32.31	1.19	2.79	0.241

Table 6 Calculated equilibrium film thickness, interfacial tension and Hamaker constant based on 1 M sodium chloride solution for Jung and Wan (2012) experimental data

Pressure-MPa	Contact angle-degrees	Interfacial tension-mN/m	Hamaker constant	pH	Film thickness-nm
7	45	42.50	$-9.57 * 10^{-22}$	2.91	0.076
7.25	52	41.93	$-9.50 * 10^{-22}$	2.90	0.071
7.3	55	41.81	$-9.47 * 10^{-22}$	2.90	0.045
15	57	35.58	$5.37 * 10^{-20}$	2.69	0.035

Table 7 Calculated equilibrium film thickness calculation, interfacial tension and Hamaker constant based on 1 M sodium chloride solution for Jafari and Jung (2018) experimental data

Pressure-MPa	Contact angle-degrees	Interfacial tension-mN/m	Hamaoka constant-J * 10^{-21}	pH	Film thickness-nm
5	88	48.89	− 2.83	3.86	0.033
7.8	87.5	40.79	− 2.26	3.43	0.034
10	66.6	37.48	− 1.23	3.27	0.098
15	41.5	34.71	1.71	3.11	0.013

disjoining pressures are repulsive and decreasing in magnitude. For both cases, Hamaker constant is positive at the maximum pressure, which translates to attractive van der Waals repulsion. For the experimental data of Chen et al. (2015), Hamaker constants are positive at all pressures and pH values, implying attractive van der Waals disjoining pressure forces leading to a consistent decrease in equilibrium water film thickness as seen in Table 5. This also agrees with the observed decrease in equilibrium film thickness with contact angle increase (Kim et al. 2010). Under conditions of elevated pressure, temperature and salinity commonly encountered in geological carbon storage, the thickness of the water film is less than 10 nm (Tokunaga 2012), which is theoretically confirmed by the solution to Eq. (11) in the present study, given that experimental data were acquired under similar conditions.

For Tables 5, 6 and 7, calculated interfacial tensions using Eq. (22) decrease with pressure at the given salinity and temperature for the carbon dioxide–brine system, similar to that reported in the literature (Bachu and Bennion 2009; Chalbaud et al. 2010). For thin film thickness calculation using Eq. (11), the point of zero charge pH of mica was taken as 2 (Filipov et al. 2012), which is different from that (3.64) obtained by Amadu and Miadonye (2022) based on contact angle versus pH plot. The difference in point of zero charge pH stems from the fact that there are different types of micas (Michaud 2016), each with its crystal chemistry that affects point of zero charge pH (Sverjensky 1994).

The enhanced water wettability of quartz compared to mica is known in the literature (Jung and Wan 2011), which is due to higher concentration of Silanol group on the former. Moreover, the more wetting the substrate, which is indicated by lower values of contact angle, the thicker the thin wetting film (Huhtamäki et al. 2018). Therefore, based on the differences in the surface chemistry of substrates, the variation of the thin wetting film as shown in Tables 5, 6 and 7 can be explained as follows:

For the silica systems studied in this paper, the thin wetting films for Chen et al. (2015) will be averagely higher compared to those of Jung and Wan (2012), and this observation is applicable as seen in Tables 5 and 6, given the higher values of contact angles for the latter system. On the basis of surface chemistry, the higher concentration of silanol group on silica means that the thin wetting film on mica will be averagely lower than those of silica and this is evident in Table 7 for the mica system.

Table 8 Calculated solubility and film thickness for the present work, and experimental contact angle data for mica–brine–carbon dioxide system for 1 M sodium chloride solution based on Jung and Wan (2012) experimental data

Pressure-MPa	Calculated carbon dioxide solubility-mol/L	Calculated pH	Contact angle from Appendix 1	Equilibrium film thickness-nm
7	0.46255	2.91	45	0.076
7.25	0.4856	2.90	52	0.071
7.3	0.4912	2.90	55	0.045
15	1.293067	2.69	57	0.035

Table 9 Calculated solubility and film thickness for this work and contact angle data for quartz–brine–carbon dioxide system for 1 M sodium chloride solution based Chen et al. (2015) experimental data

Pressure-MPa	Calculated carbon dioxide solubility-mol/L	Calculated pH	Contact angle from Appendix 3	Calculated equilibrium film thickness-nm
7	0.05890	3.34	21.85	0.797
8	0.09285	3.26	22.5	0.277
9	0.1336	3.18	23	0.273
10	0.1812	3.12	23.75	0.269
12	0.2967	3.01	23.85	0.244
18	0.8066	2.79	23.92	0.276

Table 10 Calculated solubility and film thickness for this work, and contact angle data for mica–brine–carbon dioxide system for 1 M sodium chloride solution based Jafari and June experimental data (Jafari and Jung 2018)

Pressure-MPa	Calculated carbon dioxide solubility-mol/L	Calculated pH	Contact angle from Appendix 2	Equilibrium film thickness-nm
3	0.009	3.91	79	0.033
5	0.114	3.86	88	0.034
7.8	0.0855	3.43	87.5	0.098
10	0.1812	3.27	66.5	0.013
13	0.3647	3.11	41.5	0.033

Correlation of equilibrium film thickness to pH

Tables 8, 9 and 10 shows calculated carbon dioxide solubility using Eqs. (12) and (13), pH, pressure, contact angle and equilibrium thickness. In all cases, as pressure increases, the solubility of carbon dioxide increases along side dissolution at a given temperature and salinity of brine. Consequently, the pH decreases, causing dewetting or contact angle increase (Jung and Wang 2012) in line with the experimental findings of Tokunaga (2012). The increase of film thickness with contact angle decreases which corresponds to trends related to pressure decrease in the present study has also been experimentally confirmed (Ali et al. 2019).

The van der Waals jump decreases with increasing pH as ionic strength remains constant (Zachariah et al. 2016). Debye length is not changing with pH when ionic strength is kept constant, and this is an effect of surface potential/charge density. The surface potential is more negative at higher pH, which strengthens repulsive Electric Double Layer (EDL) forces at small distances. Consequently, decreasing surface charge density due to acidification (pH decrease) of carbon dioxide equilibrated brine at pressure, salinity and temperature conditions compresses the electric double layer, which causes film thinning.

Tables 8, 9 and 10 shows calculated solubility versus pressure at a salinity of 1 M sodium chloride solution at a temperature of 318 K. In all cases, carbon dioxide solubility calculated using Eqs. (12) and (13) show increase. Accordingly, the pH calculated using Eq. (14) decreases due to the salinity and temperature dependence of the ionization constant (Eq. 17). The increase in pressure also causes contact angle increase due to pH decrease (Virga et al. 2018).

Correlation of the electrokinetic properties of minerals to aqueous pH and film thickness

Since surface charge density/potential is related to aqueous pH and the electrokinetic properties of substrates, there must be a correlation between the equilibrium film thickness and

these parameters, given the dependence of EDL repulsion on them. Generally, the surface charge on a substrate at a given pH depends on the point of zero charge pH. Above the point of zero charge pH, the substrate develops a negative charge. Accordingly, it develops a positive charge below the point of zero charge pH (Kosmulski and Mączka 2021). The minerals studied in this paper are quartz and muscovite mica. The point of zero charge pH of quartz is on the average 3 (Amadu and Midonye 2017). The point of zero charge pH of muscovite mica was assumed as 2 in this study (Filippov et al. 2012). Zeta potential is linked to the electrokinetic properties of the substrate. The square of the zeta potential is proportional to the force of electrostatic repulsion between charged particles and will, therefore, affect the equilibrium film thickness. Normally, increasing the absolute zeta potentials increases electrostatic stabilization. Consequently, as the zeta potential approaches zero, electrostatic repulsions become small compared to the ever-present van der Waals attraction. Eventually, instability increases, which can result in equilibrium film thinning.

Recently, Hidayat et al. (2022) reported empirical relationships that describe the pH dependence of the zeta potential that provides an essential insight into interfacial electrochemistry of silica-water systems at conditions relevant to carbon dioxide geological sequestration. The following is the relationship:

$$\zeta_M(\mathrm{mV}) = -4.86 * \mathrm{pH} + 12.57 \tag{24}$$

The correlation has a regression coefficient of 0.976.

From Table 7 for Jafari and Jung (2018), film thickness increases sharply at pH 3.11 to 0.013 nm. At this pH, the surface of mica is negatively charged, given its point of zero charge pH equal to 2. The zeta potential of the carbon dioxide–brine interface will be − 15.11 based on Eq. (24). Consequently, there is double layer repulsion. At this pH, the Hamaker constant is positive, indicating van der Waals attractive disjoining pressure. However, double layer repulsion is weak due to high electrolyte concentration leading to the sharp decrease in film thickness from 0.098 to 0.013 nm as seen from calculation. Therefore, in Table 7, the electrokinetic property of muscovite mica guaranteed negative zeta potentials/negative surface charge density/potentials for all aqueous pH in addition to similar electrical properties at the CO_2–brine interface, but double layer repulsion is weak which, coupled with decreasing van der Waals repulsion caused a gradual decrease in equilibrium film thickness.

Unlike van der Waals forces, double layer forces are sensitive to pH and salinity of the aqueous phase and can be attractive (Tadros, 2013) or repulsive (Munday and Capasso, 2010). Generally, the overlap of the electrical double layers of similar electrostatic polarity leads to repulsive forces at low salt concentrations, which transcend the attractive van der Waals forces, giving rise to equilibrium film stability as has been observed in colloidal systems (Pavlovic et al. 2016). The double layer forces weaken progressively with the increasing electrolyte level due to surface charge screening by the salts. In addition, anion adsorption on the positively charged surface leads to reduced surface charge density, and hence, to weaker double layer forces. In the present study, the 1 M sodium chloride aqueous solution has a higher concentration, and the force profile is entirely dominated by the attractive van der Waals force (Smith et al. 2019). Moreover, considering Jung and Wan (2012) experimental data calculated corresponding pH, the zeta potential of the brine–CO_2 interface will be negative for the pressure range reported. At the same time, considering the point of zero charge pH of silica to be 3, the surface of silica will be barely positively charged. The implication is that there will be double layer attraction/disjoining pressure, while the negative value of Hamaker constant translates to repulsive van der Waals forces, which decreases with pressure increase, causing decreased film thickness as seen from calculations. Accordingly, at a pressure of 15 MPa, the Hamaker constant is positive, implying attractive van der Waals repulsion, which together with attractive double layer repulsion cause a further decrease in film thickness as seen in Table 6.

For Chen et al. (2015) experimental data, the zeta potential of the CO_2-interface decreases from large negative at a lower pressure to small negative at the highest pressure as seen in Table 9. At the same time, the negatively charged silica–brine interface decreases dues to pH decrease in accordance with pH dependent surface charge regulation (McBride 1989). Consequently, double layer repulsion, coupled with the high salinity condition decreases. Also, the positive values of the Hamaker constant for all pressures imply van der Waals attractive repulsion. Consequently, both double layer and van der Waals forces favor equilibrium film thinning as seen in Table 7 for Jafarai and Jung experimental data.

In a molecular dynamic simulation study (Sun and Bourg 2020), the values of disjoining pressure were grouped into three ranges of gas pressure, including dilute gas for gas pressure = 0–2.5 Mpa, dense gas for gas pressure = 5.4–6.8 Mpa, and supercritical fluid for gas pressure greater than 7.9 Mpa. For supercritical carbon dioxide, disjoining pressure went from positive to negative values for a system with partial wetting ($\theta > 0$) (Kuchin and Starov 2015). This observation for the supercritical carbon dioxide case is seen in Tables 6 and 7 for Jung and Wang (2012) and Jafari and Jung (2018), respectively, as dominant van der Waals disjoining pressure goes from positive values due to negative values of Hamaker constant to a positive value at maximum pressure. The following section will be devoted toward validation

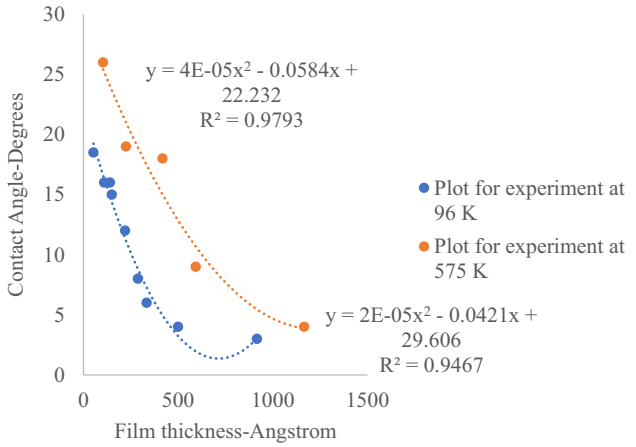

Fig. 2 Plot of contact angle versus film thickness based on experimental data from Slep et al. (2000) (96 K = 96,000 g/mole; 575 K = 575,000 g/mole of polystyrene substrate)

of the model calculations against experimental data in the literature.

Model validation against litereature work

The theory of the effect of intermolecular forces on wetting film thickness and contact angle is universal and applies not only to the carbon dioxide–brine solid systems (Slep et al. 2000; Fenistein, et al. 2002; Pahlavan et al. 2018; Mazzoco and Wayner Jr 1999; Habibi and Dehghanpour 2018). In all cases, the effect of intermolecular forces is quantified in the form of disjoining pressure force components that were principal to the rigorous derivation of the model. Consequently, experimental data on equilibrium wetting film thickness versus equilibrium contact angle provide the basis for validating model calculations. In this regard, the experimental data of Slep et al. (2000) was used to check the validity of model calculations of thin wetting film thickness. In this cited literature, the authors provided experimental data on equilibrium contact angle versus equilibrium wetting film thickness. To validate the model, polynomial curves were fitted to the plots of their data. Similar plats wre then carried out of calculated contact angle versus film thickess. Consequently, Fig. 2 shows plots for literature based experimental data, while Figs. 3, 4 and 5 shows plots for the data.

In the carbon dioxide–brine–solid system, pH is the principal cause of contact angle changes following carbon dioxide injection and dissolution in formation brine. Consequently, the existence of the point of zero charge pH of the solid surface implies maximum dewetting where contact angle is a maximum at this pH and lower at a pH lower and above this pH (Carré et al. 2003). This trend is due to the fact that above the point of zero charge pH, the surface develops a negative surface charge density, while below this point, it develops a positive surface charge density (Churchill et al. 2004) with the potential to affect the equilibrium contact angle accordingly. Consequently, a plot of wetting film thickness versus contact angle where a parabolic fit is invoked is found appropriate in this research work.

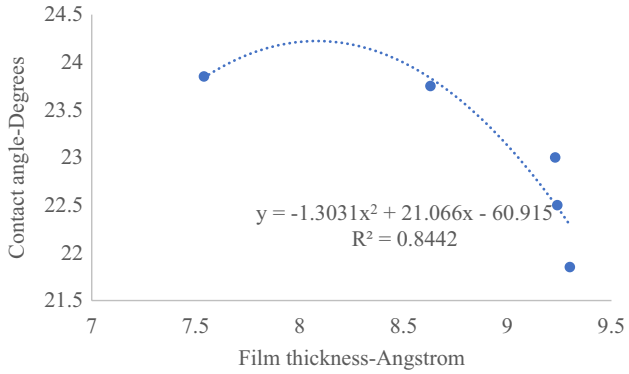

Fig. 3 Plot of contact angle versus film thickness based on calculations using the model and data from Chen et al. (2015)

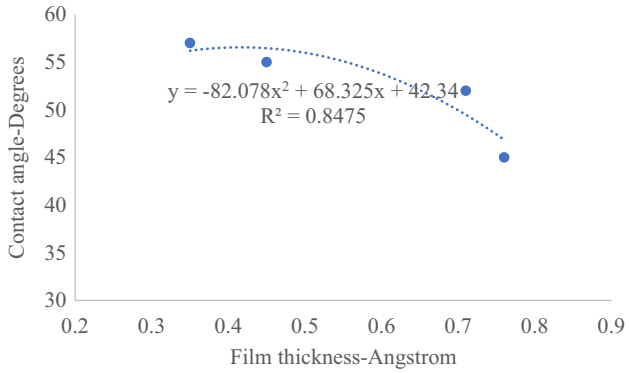

Fig. 4 Plot of contact angle versus film thickness based on calculations using the model and data from Jung and Wan (2012)

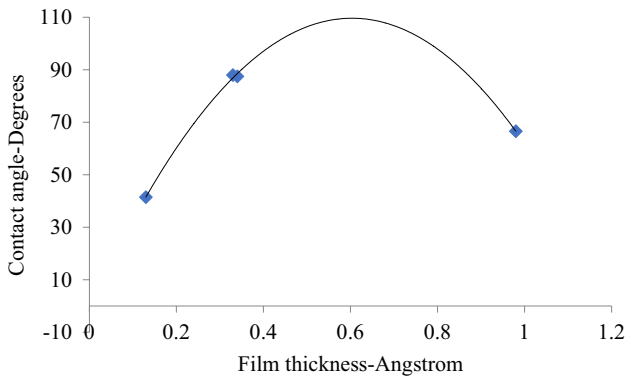

Fig. 5 Plot of contact angle versus film thickness based on calculations using the model and data from Jafari and Jung (2018)

Accordingly, the regression coefficient for polynomial fit to calculated film thickness versus contact angle angle are 0.84, 0.85 and almost one for Figs. 3, 4 and 5, respectively, with an average value of 0.89, while the average values for coefficeints in Fig. 4 is 0.96 corresponding to a difference of 0.08. Therefore, the model calculates film thickness with a resonable degree of certainty, given the slight deviation as seen from comaparison of the regression coefficients.

In foam systems, solution to the linear problem for the evolution of the fluctuations in the local film thickness has been used to understand film stability. The approach allows to calculate the critical thickness at which the system becomes unstable (Valkovska et al. 2000) In this regard, the critical wave number depends only on the disjoining pressure and surface tension, and the final form of the theoretical approach leads to a transcendental equation for the critical film thickness. Perovich et al. (2014), have studied the problem of finding an exact analytical closed-form solution of some families of transcendental equations, which describe the equilibrium critical thickness of epitaxial thin films. While the cited research works deal solely with transcendental equations applied to research works concerning film thickness not related to wettability issues, the present study, through its rigorous mathematical approach, has related transcendental equations to thin films dealing with the wettability of the carbon dioxide–brine–solid systems.

Summary and conclusions

A macroscopic model based on the phenomenological Young's equation and the geometric mean method for interfacial tension, and long-range van der Waals intermolecular interaction correctly predicts the trend and magnitude of contact angle dependence on pressure (Li et al. 2007). Consequently, by integrating the electric double layer concept, the concept of disjoining pressure relationship to the thin wetting film in the system carbon dioxide–brine–solid permits application of the Frumkin–Derjaguin (FD) equation for the theoretical calculation of the thin water film. Herein, the thickness of the equilibrium water film was obtained based on the substitution of the van der Waals and double layer repulsion models into the FD equation, followed by a rigorous derivation of a transcendental equation that links film thickness to experimentally accessible parameters. Saline aquifer depth-dependent CO_2 and water properties were used to calculate Hamaker constants for water film on silica and mica to facilitate determination of film thickness by analytical solution to the derived equation. The effect of short range hydration forces was neglected in accounting for total disjoining pressure in the derivation of film thickness equation partly due to its poorly understood nature and partly due to the high salinity of the aqueous system studied in this work. The development of the thin wetting film can be likened to an imbibition phenomenon, where a momentary temperature rise due to heat transfer can occur (Aslannejad et al. 2017) due to similarity to imbibition under temperature effect (Amadu and Pegg 2019). In this paper, the effect of heat transfer on the thin wetting film was neglected. The possible effect of heat was also not account for. The following conclusions are derived from this study:

1. The original Frumkin–Derjaguin equation provides a theoretical basis for the derivation of a transcendental equation that expresses the equilibrium thin film as a function of equilibrium contact angle, pH of aqueous solution, temperature and salinity and this has been demonstrated in this work.
2. Calculated thin film thicknesses based on the derived equation in this study agree with experimentally observed film thicknesses in the literature.
3. Following the theoretical agreement of the derived equation with experimental observations, this study supplements experimental approaches based on Molecular Dynamic Simulations for the determination of the thin water film thickness for the carbon dioxide–brine–solid system.
4. Under conditions commonly encountered in geological carbon storage, the thickness of the water film is less than 10 nm (Tokunaga 2012) and this has been theoretically confirmed by this work.
5. Negative values of the Hamaker constant encountered in the carbon dioxide–brine–mineral systems have also been obtained in the present work based on theoretical calculations employing the fundamental equation of Lifshitz macroscopic theory (Takagish et al. 2019) that uses the macroscopic parameters of dielectric permittivity and refractive index of interacting media.
6. The carbon dioxide–brine interfacial tension is critical for calculating the equilibrium thin film thickness using the model derived from the Frumkin–Derjaguin equation. A universal model for calculating this parameter was used for testing the model. The implication is that the model provides a reliable basis for calculation, given the consistency of the results compared to literature reported values.
7. The study links for the first time, a transcendental equation to the thin wetting film for the carbon dioxide–solid–brine system encountered in geological carbon storage.

Appendix 1. Experimental data for silica–carbon dioxide–brine system

The entire system was enclosed in a temperature-controlled glove box maintained at the constant temperature of 45 ± 1 °C during experiment (Courtesy of Jung and Wan 2012).

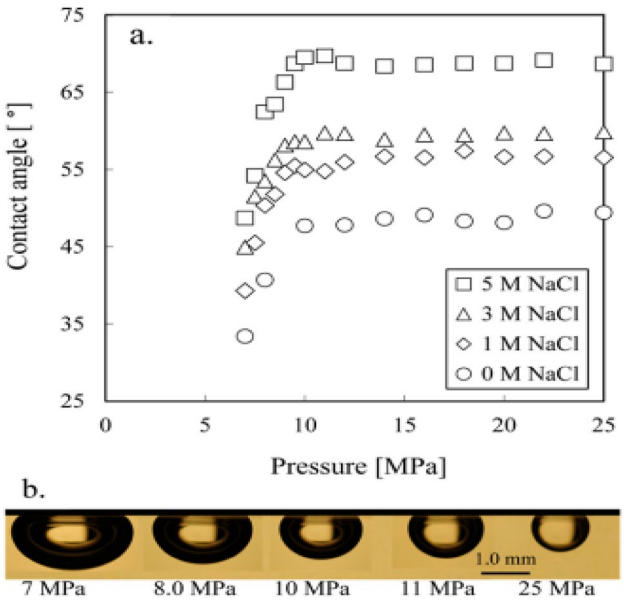

Appendix 2: Experimental data for mica–carbon dioxide–brine: variations of and initial contact angle with pressure; a Type V5 with deionized water, b V1 with deionized water, c Type V5 with1 M NaCl, d Type V1 with 1 M NaCl, d Type V5 with 3 M NaCl, e Type V1 with 3 M NaCl (Courtesy of Jafari and Jung 2018).

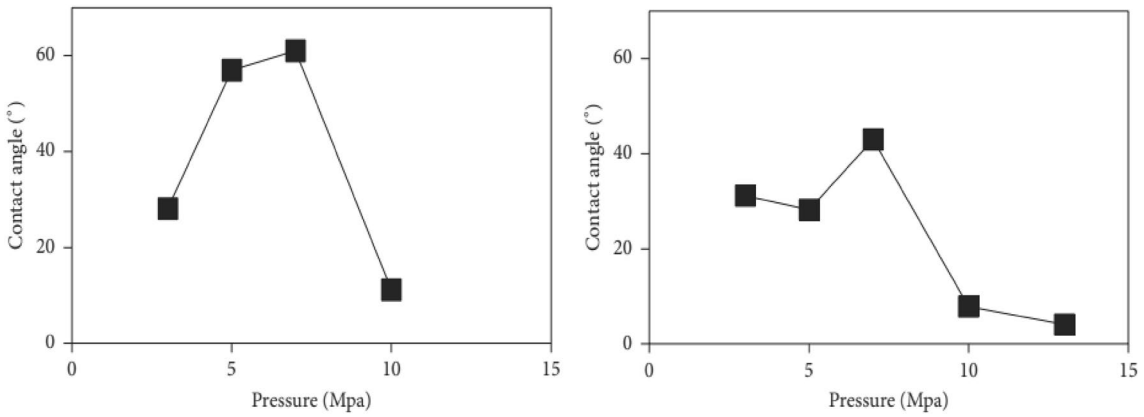

Appendix 3: Experimental data for quartz–carbon dioxide–brine systems for water contact angles on quartz surface as a function of system pressure when ionic concentration is 1 M and temperature is 318 K for monovalent and divalent ions. Right bottom: photographs of CO_2 droplet on quartz surface during static contact angles measurement. A scale bar of 1 mm was shown (Courtesy of Chen et al. 2015).

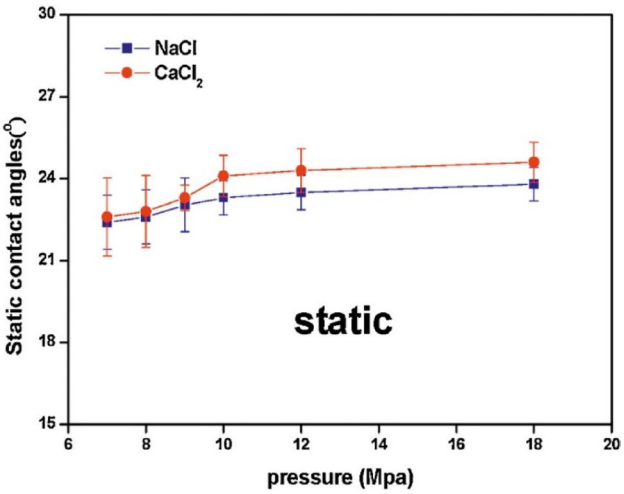

Appendix 4. CO_2 relative permittivity (Courtesy of Michels and Michels 1933)

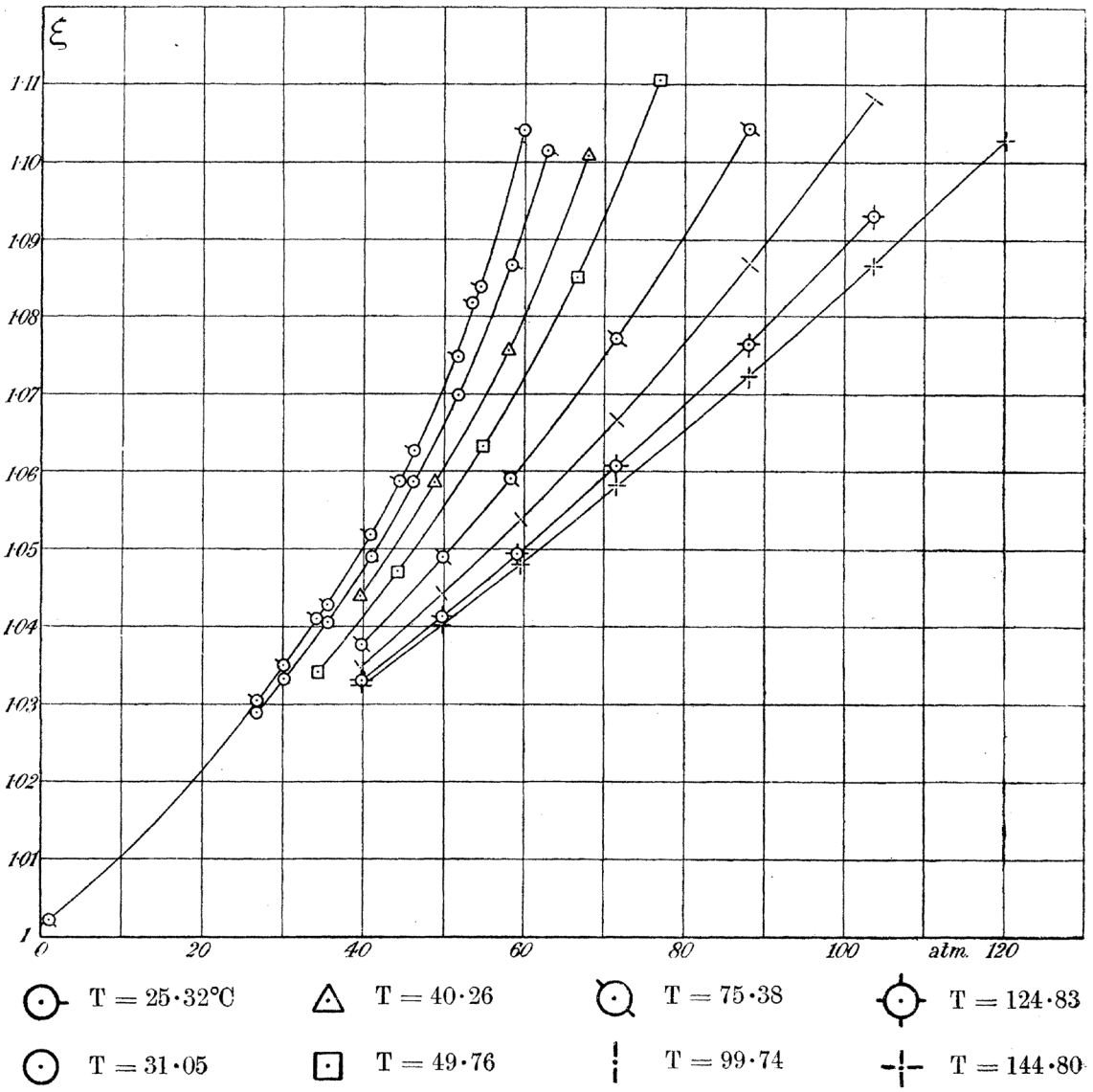

Acknowledgements The authors wish to greatly acknowledge the Office of Research and Graduate Studies of Cape Breton University for its research support that enables us to carry out this project. The support of Cape Breton University Library is also appreciated for the literature materials. Finally, Dr. D.J.G. Irwin's role in editing the manuscript is also greatly acknowledged.

Funding This research was funded by Cape Breton University Office of Research and Graduate Studies.

Declarations

Conflict of interest All authors wish to declare that there is no conflict of interest in this research work.

References

Afzal S, Tesler W, Blessing S, Collins J, Lis L (1984) Hydration force between phosphatidylcholine surfaces in aqueous electrolyte solutions. J Colloid Interface Sci 97(2):303–307

Aggelopoulos CA, Robin M, Vizika O (2011) Interfacial tension between CO2 and brine (NaCl + CaCl2) at elevated pressures and temperatures: the additive effect of different salts. Adv Water Res 34(4):505–511

Aissa MF, Bahloul S, Le-Bail A (2015) Effect of temperature on the solubility of CO2. Int J Food Prop 18:1097–1109

Ali N, Addali A, Teixeira JA (2019) Effect of water temperature, pH value, and film thickness on the wettability behaviour of copper surfaces coated with copper using EB-PVD technique. J Nano Res 60:124–141

Altamirano MÁ, Pérez E, Goicochea AG (2016) On finite size effects, ensemble choice and force influence in dissipative particle dynamics simulations. In: High performance computing, vol 697, pp 314–328

Amadu M, Miadonye A (2019a) Derivation of a pH dependent solid–liquid interfacial tension and theoretical interpretation of the physicochemistry of dewetting in the CO2-brine-silica system. Int J Chem 11(2):127–155

Amadu M, Miadonye A (2019b) Modeling of contact angle versus pH and derivation of contact angle versus pressure in deep saline aquifers under geological carbon storage. Int J Chem 12(2):19–34

Amadu M, Midonye A (2022) Applicability of the linearized Poisson–Boltzmann theory to contact angle problems and application to the carbon dioxide-brine-solid systems. Sci Rep 12(1):1–19

Amadu M, Pegg MJ (2019) Analytical solution to spontaneous imbibition under vertical temperature gradient based on the theory of spontaneous imbibition dynamics. J Pet Sci Eng 172:627–635

Amadu, Mumuni and Miadonye, Adango (2017) Determination of the Point of Zero Charge pH of Borosilicate Glass Surface Using Capillary Imbibition Method. Int J Chem 9(3):1–18

Aram KFL, Mugele F, Siretanu I (2022) Correlation between electrostatic and hydration forces on silica and gibbsite surfaces: an atomic force microscopy study. Langmuir 38(3):914–926

Aslannejad H, Terzis A, Hassanizadeh M, Weigand B (2017) Occurrence of temperature spikes at a wetting front during spontaneous imbibition. Sci Rep 7(7268):1–15

Bachu S, Bennion DB (2009) Interfacial tension between CO2, freshwater, and brine in the range of pressure from (2 to 27) MPa, temperature from (20 to 125) °C, and water salinity from (0 to 334 000) mg·L-1. J Chem Eng Data 54:765–775

Badera A, Thibeau S, Vincké O, Jannaud D, Saysset S, Joffre GH, Giger FM, David M, Gimenez M, Dieulin A, Copin D (2014) CO2 storage capacity evaluation in deep saline aquifers for an industrial pilot selection. Methodology and results of the France Nord Project. Energy Procedia 63:2779–2788

Bahadori A, Vuthaluru HB, Mokhatab S (2009) New correlations predict aqueous solubility and density of carbon dioxide. Int J Greenh Gas Control 3:474–480

Bergeron V (1997) Disjoining pressures and film stability of alkyltrimethylammonium bromide foam films. Langmuir 13:3474–3482

Bergström L (1997) Hamaker constants of inorganic materials. Adv Colloid Interface Sci 70:125–169

Bonto M, Eftekhari AA, Nick HM (2019) An overview of the oil-brine interfacial behavior and a new surface complexation model. Sci Rep 9(6072):1–16

Boström M, Williams DR, Ninham BW (2001) Specific ion effects: why DLVO theory fails for biology and colloid systems. Phys Rev Lett 87(16):168103

Bowles AP, Hsia Y-T, Jones PM, White LR, Schneider JW (2009) Quasi-equilibrium AFM measurement of disjoining pressure in lubricant nanofilms II: effect of substrate materials. Langmuir 25(4):2101–2106

Carré A, Lacarrière V, Birch W (2003) Molecular interactions between DNA and an aminated glass substrate. J Colloid Interface Sci 260(1):49–55

Chairman FB, Schairer J, Spicer HC (1942) Handbook of physical constants. The Geological Soceity of America

Chalbaud C, Robin M, Lombard JM, Martin F, Egermann P, Bertin H (2009) Interfacial tension measurements and wettability evaluation for geological CO2 storage. Adv Water Res 32(1):98–109

Chalbaud C, Robin M, Lombard J-M, Bertin H, Egermann P (2010) Brine/CO2 interfacial properties and effects on CO2 storage in deep saline aquifers. Oil Gas Sci Technol Rev IFP 65(4):541–555

Chen C, Wan J, Li W, Song Y (2015) Water contact angles on quartz surfaces under supercritical CO2 sequestration conditions: experimental and molecular dynamics simulation studies. Int J Greenh Gas Control 42:655–665

Chen C, Song Y, Li W (2016) Wettability-water/brine film thickness relationship and the effect of supercritical CO2 pre-contact for CO2/brine/mineral systems under geologic CO2 sequestration conditions: insights from molecular dynamics simulations. American Geophysical Union, Fall Meeting. AGU

Churchill H, Teng H, Hazen RM (2004) Correlation of pH-dependent surface interaction forces to amino acid adsorption: implications for the origin of life. Am Miner 89:1048–1055

Clergen Y, Durou C, Laurens M (1999) Refractive index variations for argon, nitrogen and carbon dioxide at $\lambda = 632.8$ nm (He–Ne laser light) in the range 288.15 K e T e 323.15 K, $0 < p < 110$ kPa. Chem Eng J 44(2):197–199

Condon JB (2006) Chapter 4—theories behind the Chi plot. In: Surface area and porosity determinations by physisorption physisorption{ measurements and theory. Elsevier, pp 91–125

Daniels DJ (1996) Surface-penetrating radar—IEE radar, sonar, navigation and avionics, vol 6. The Institue of Electrical Engineers, p 320

Evans DF, Wennerstöm H (1999) The colloidal domain. Wiley

Exerowa D, Platikanov D, Levecke B, Tadros T (2009) Emulsion and wetting films stabilized by hydrophobically modified inulin polymeric surfactant. J Dispers Sci Technol 30:789–794

Fenistein D, Bonn D, Rafaı S, Wegdam GH, Meunier J, Parry AO, Gama MM (2002) What controls the thickness of wetting layers near bulk criticality? Phys Rev Lett 89(9):1–4

Fiedler M (1994) Numerical solution of algebraic and transcendental equations. Springer

Filippov L, Duverger A, FilippovaInna I, Kasaini H, Thiry J (2012) Selective flotation of silicates and Ca-bearing minerals: the role of non-ionic reagent on cationic flotation. Miner Eng 36–38:314–323

Fukuzawa K, Kawamura J, Deguchi T, Zhang H, Mitsuya Y (2004a) Disjoining pressure measurements using a microfabricated groove for a molecularly thin polymer liquid film on a solid surface. J Chem Phys 121(9):4358–4363

Fukuzawa K, Kawamura J, Deguchi T, Zhang H, Mitsuya Y (2004b) Measurement of disjoining pressure of a molecularly thin

lubricant film by using a microfabricated groove. IEEE Trans Magn 40(4):3183–3185
Gaebel C, Lead JR, Renshaw JC, Tellam JH (2009) Indications from atomic force microscopy of the presence of rapidly formed nanoscale films on aquifer material surfaces. J Contam Hydrol 108(1–2):46–53
Habibi A, Dehghanpour H (2018) Wetting behavior of tight rocks: from core scale to pore scale. Water Resour Res 54(11):9162–9186
Hamilton A, Koutsosa V, Halla C (2010) Direct measurement of salt–mineral repulsion using atomic force microscopy. Chem Commun 46:5235–5237
Hamm LM, Bourg IC, Wallace AF, Rotenberg B (2013) Molecular simulation of CO2-and CO3-brine-mineral systems. Rev Mineral Geochem Mineral Soc 77(1):189–228
Hidayat M, Sarmadivaleh M, Derksen J, Vega-Maza D, Iglauer S, Vinogradov J (2022) Zeta potential of CO2-rich aqueous solutions in contact with intact sandstone sample at temperatures of 23 C and 40 C and pressures up to 10.0 MPa. J Colloid Interface Sci 607:1226–1238
Hirasaki G (1991) Wettability fundamentals and surface forces. SPE Form Eval 6(2):217–226
Huhtamäki T, Tian X, Korhonen JT, Ras RH (2018) Surface-wetting characterization using contact-angle measurements. Nat Protoc 13:1521–1538
IFTI (2018) International Fireproof Technology Inc. Retrieved from the ultimate in firestop solutions and fire protective coatings. https://painttoprotect.com/wp-content/uploads/2018/05/how-to-use-wet-film-gauge-dc315-eng.pdf
Israelachvili JN (2011) In intermolecular and surface forces, 3rd edn. Elsevier
Jafari M, Jung J (2018) Variation of contact angles in brine/CO2/mica system considering short-term geological CO2 sequestration condition. Geofluids 2018:1–15
Jeswal S, Chakraverty S (2018) Solving transcendental equation using artificial neural network. Appl Soft Comput 73:562–571
Jones PM, Luo M, White L, Schneider J (2005) Measurement of disjoining pressure of Z-type perfluoropolyether lubricants on Si and SiNx surfaces. Tribol Int 38(6–7):528–532
Jones DA (2005) Understanding microwave treatment of ores. Ph.D. thesis, University of Nottingham
Jung J, Wan J (2011) Wettability alteration upon reaction with scCO2: silica, mica, and calcite. In: AGU fall meeting, vol, 2011,V14A-07
Jung J-W, Wan J (2012) Supercritical CO2 and ionic strength effects on wettability of silica surfaces: equilibrium contact angle measurements. Energy Fuels 26:6053–6059
Kano Y, Kuramoto N (2021) Gaseous density calculation by means of relative permittivity measurement. Meas Sens 18:1–4
Karakashev S, Stöckelhuber K, Tsekov R, Phan C, Heinrich G (2014) Tribology of thin wetting films between a bubble and a moving solid surface. Adv Colloid Interface Sci 210:39–46
Kelemen P, Benson SM, Pilorgé H, Psarras P, Wilcox J (2019) An overview of the status and challenges of CO2 storage in minerals and geological formations. Front Clim 15:1–20
Kennedy CD (1990) Ionic strength and the dissociation of acids. Biochem Educ 18(1):35–40 (**Retrieved from Biochemical Education**)
Kesler V, Murmann B, Soh HT (2020) Going beyond the Debye length: overcoming charge screening limitations in next-generation bioelectronic sensors. ACS Nano 14(12):16194–16201
Kim H-M, Jang J, Sohn S (2010) Super-hydrophobicity of PTFE films coated on an etched Al surface by using a RF-magnetron sputtering method. J Korean Phys Soc 57(5):1281–1284
Kim Y, Wan J, Kneafsey TJ, Tokunaga TK (2012) Dewetting of silica surfaces upon reactions with supercritical CO2 and brine: pore-scale studies in micromodels. Environ Sci Technol 46(7):4228–4235
Kim TW, Tokunaga TK, Shuman DB (2012) Thickness measurements of nanoscale brine films on silica surface under geologic CO2 sequestration conditions using synchrotron X-ray fluorescence. Water Resour 48:1–13
Kosmulski M, Mączka E (2021) The isoelectric point of an exotic oxide: tellurium (IV) oxide. Molecules 26(11):1–11
Kuchin I, Starov V (2015) Hysteresis of contact angle of sessile droplets on smooth homogeneous solid substrates via disjoining/conjoining pressure. Langmuir 31:5345–5352
Kuchin I, Matar O, Craster R, Starov V (2014) Influence of the disjoining pressure on the equilibrium interfacial profile in transition zone between a thin film and a capillary meniscus. Colloids Interface Sci Commun 1:18–22
Lee S-W, Wolfgang S (2001) Repulsive van der Waals forces for silica and alumina. J Colloid Interface Sci 243:365–369
Li Y, Pham JQ, Johnston KP, Green PF (2007) Contact angle of water on polystyrene thin films: effects of CO2 environment and film thickness. Langmuir 23:9785–9793
Li X, Boek E, Maitland GC, Trusler JP (2012) Interfacial tension of (brines + CO2): (0.864 NaCl + 0.136 KCl) at temperatures between (298 and 448) K, pressures between (2 and 50) MPa, and total molalities of (1 to 5) mol·kg−1. J Chem Eng Data 57:1078–1088
Liu S, Yang X, Qin Y (2021) Molecular dynamics simulation of wetting behavior at CO2/water/solid interfaces. Chin Sci Bull 55(21):2252–2257
Luck R, Zdaniuk GJ, Cho H (2015) An efficient method to find solutions for transcendental equations with several roots. Int J Eng Math 2015:1–4
Malmberg C, Mariyott AA (1965) Dielectric constant of water from 0–100 celsius. J Res Nat Bur Stand 56:1–8
Mazzoco R, Wayner P Jr (1999) Aqueous wetting films on fused quartz. J Colloid Interface Sci 214(2):156–169
McBride M (1989) Surface chemistry of soil minerals. In: Dixon JB, Weed SB (Eds) Minerals in soil environments. SSSA book series no. 1, 2nd ed, pp 35–88
Michaud LD (2016) Mica mineral types. Retrieved from 911-Metallurgist: https://www.911metallurgist.com/blog/mica-mineral-types
Michels A, Michels C (1933) The influence of pressure on the dielectric on the dielectric constant of carbon dioxide up to 1000 atmospheres between 25° and 150° CA. MICHELS and Mrs. Philos Trans R Soc Lond 231:409–434
Misra RP, de Souza P, Blankschtein D, Bazant MZ (2019) Theory of surface forces in multivalent electrolytes. Langmuir 35:11550–11565
Munday, Jeremy N, Capasso, Federico (2010) Repulsive Casimir and van der Waals forces: From measurements to future technologies. Int J Mod Phys A 25(11):1–9
Nesse WD (2000) Introduction to mineralogy. Oxford University Press, New York
Ninham BW, Parsegian VA (1970) Van der Waals forces. Special characteristics in lipid-water systems and a general method of calculation based on the Lifshitz theory. Biophys J 10(3):646–663
Ohshima H (2014) Interaction of colloidal particles-Chapter 1. In: Interaction of colloidal particles in colloid and interface science in pharmaceutical research and development. Elsevier, pp 1–28
Pahlavan A, Cueto-Felgueroso L, Hosoi AE, McKinley GH (2018) Thin films in partial wetting: stability, dewetting and coarsening. J Fluid Mech 845:642–681
Pavlovic M, Huber R, Adok-Sipiczk M, Nardinab C, Szilagy I (2016) Ion specific effects on the stability of layered double hydroxide colloids. Soft Matter 12:4024–4033

Perovich S, Simic S, Tosic D, Bauk S (2007) On the analytical solution of some families of transcendental equations. Appl Math Lett 20(5):493–498
Perovich SM, Calasan MP, Toskovic R (2014) On the exact analytical solution of some families of equilibrium critical thickness transcendental equations. AIP Adv 4(117124):1–8
Radoev B, Stöckelhuber KW, Letocart P (2007a) Wetting film dynamics and stability. Colloids Interface Sci 3:151–172
Radoev B, Stöckelhuber KW, Tsekov R, Letocart P (2007b) Wetting film dynamics and stability. Colloids Interface Sci 3:151–172
Reddi LB (2011) Geological storage of carbon dioxide in baslat. IEA
Rusanov AI (2020) On the Thermodynamics of Thin Films. The Frumkin–Derjaguin Equation, Colloid Journal, 82(1):62–68.
Saraji S, Goual L, Piri M, Plancher H (2013) Wettability of supercritical carbon dioxide/water/quartz systems: simultaneous measurement of contact angle and interfacial tension at reservoir conditions. Langmuir 29:6856–6866
Sebastian MT (2008) Chapter two—measurement of microwave dielectric properties and factors affecting them. In: Dielectric materials for wireless communication. Elsevier, pp 11–47
Shiga M, Aichi M, Sorai M (2020) Quantitative investigation on the contributing factors to the contact angle of the CO2/H2O/muscovite systems using the Frumkin–Derjaguin equation. Model Simul Geofluids Transp Reserv 2020:1–11
Slep D, Asselta J, Rafailovich MH, Sokolov J, Winesett DA, Smith AP, Ade H, Anders S (2000) Effect of an interactive surface on the equilibrium contact angles in bilayer polymer films. Langmuir 16:2369–2375
Smith AM, Maroni PM, Trefalt G, Borkovec M (2019) Unexpectedly large decay lengths of double-layer forces in solutions of symmetric. Multivalent Electrolytes Phys Chem B 123(7):1733–1740
Stanford A, Tanner J (1985) Physics for students of science and engineering. Science Direct
Stogryn A (1971) Equations for calculating the dielectric constant of saline water. IEEE Trans Microw Theory Tech 19(8):733–736
Stumm W, Morgan J (1996) Aquatic chemistry, chemical equilibria and rates in natural waters, 3rd edn. Wiley
Sun EW-H, Bourg IC (2020) Molecular dynamics simulations of mineral surface wettability by water versus CO2: thin films, contact angles, and capillary pressure in a silica nanopore. J Phys Chem C 124(46):25382–25395
Sverjensky DA (1994) Zero-point-of-charge prediction from crystal chemistry and solvation theory. Geochim Cosmochim Acta 58(14):3123–3129
Takagish H, Masuda T, Shimoda T, Maezono R, Hongo K (2019) Method for the calculation of the Hamaker constants of organic materials by the Lifshitz macroscopic approach with density functional theory. J Phys Chem A 40:8726–8733
Tadros T (2013) Van der Waals Attraction. In: Tadros, T. (eds) Encyclopedia of Colloid and Interface Science. Springer, Berlin, Heidelberg. https://doi.org/10.1007/978-3-642-2066
Tenney CM, Cygan RT (2014) Molecular simulation of carbon dioxide, brine, and clay mineral interactions and determination of contact angles. Environ Sci Technol 48(3):2035–2042
Tokunaga TK (2012) DLVO-based estimates of adsorbed water film thicknesses in geologic CO2 reservoirs. Langmuir 28(21):8001–8009
Valkovska SD, Danov DK, Ivanov BI (2000) Effect of surfactants on the stability of films between two colliding small bubbles. Colloids Surf A Physicochem Eng Asp 175(1–2):179–192
Verma Y, Vishal V, Ranjith PG (2021) Sensitivity analysis of geomechanical constraints in CO2 storage to screen potential sites in deep saline aquifers. Front Clim 3:1–22
Virga E, Spruijt E, de Vos WM, Biesheuvel PM (2018) Wettability of amphoteric surfaces: the effect of pH and ionic strength on surface ionization and wetting. Langmuir 34(50):15174–15180
Waggett F, Shafiq MD, Bartlett P (2018) Failure of Debye-Hückel screening in low-charge colloidal suspensions. Colloids Interfaces 2(51):1–9
Weeks J Jr (1922) The dielectric constant of mica. Phys Rev 19(4):319
Williams JD, Fellgett MW, Quinn MF (2016) Carbon dioxide storage in the captain sandstone aquifer: determination of in situ stresses and fault-stability analysis. Br Geol Surv 22:211–222
Yan W, Huang S, Stenby EH (2011) Measurement and modeling of CO2 solubility in NaCl brine and CO2-saturated NaCl brine density. Int J Greenh Gas Control 5(6):1460–1477
Yaros H, Newman J, Radke C (2003) Evaluation of DLVO theory with disjoining-pressure and film-conductance measurements of common-black films stabilized with sodium dodecyl sulfate. J Colloid Interface Sci 262(2):442–455
Zachariah Z, Espinosa-Marzal RM, Spencera ND, Heuberger MP (2016) Stepwise collapse of highly overlapping electrical double layers. Phys Chem Chem Phys 18:24417–24427
Zhang Y, Yang J, Yu Y-X (2005) Dielectric constant and density dependence of the structure of supercritical carbon. J Phys Chem B 109:13375–13382
Zulkifli NA, Johar MA, Faizan OM, Marwah, Ibrahim MH (2017) Review on advances of functional material for additive manufacturing. In: IOP conference series: materials science and engineering 226. IOP, pp 1–11